A Reproducible Expository Analysis of the Logistic Map: Stability, Period Doubling, Conjugacy and Symbolic Dynamics

Joshua Owolabi Adeleke
Department of Applied Mathematics
Illinois Institute of Technology
Chicago, IL 60616, USA
jadeleke@hawk.iit.edu

The logistic map is the standard first example in introductions to discrete dynamical systems, but its treatment is scattered across sources, and the numerical practice behind its familiar pictures is rarely documented. A self-contained account is assembled here. Complete derivations are given for the fixed-point and period-two stability windows, including the frequently misstated marginal parameter, where the fixed point is non-hyperbolic yet still attracting. Period-doubling thresholds are determined to 10 significant figures by a simultaneous Newton solve, and ratios formed from four-decimal thresholds are shown incapable of converging to the Feigenbaum constant. A conjugacy with the tent map is proved and combined with the itinerary map to establish that the fully developed case is chaotic in the sense of Devaney, with topological entropy and Lyapunov exponent both equal to the natural logarithm of two. The numerical tables are independently cross-checked against exact formulas, stability criteria or higher-precision computations.

Keywords: logistic map; chaos; period doubling; Feigenbaum constant; Lyapunov exponent; tent map; symbolic dynamics; reproducible numerics

1. Introduction

The logistic map

$$f_\mu(x) = \mu x(1 - x), \quad x \in [0, 1], \quad \mu \in [0, 4], \tag{1}$$

occupies an unusual position in mathematics. It is simple enough to be written on a napkin and iterated on a pocket calculator, and yet it exhibits, within a single one-parameter family, an infinite cascade of bifurcations, a universal scaling constant shared with systems that have nothing else in common with it, sensitive dependence on initial

https://doi.org/10.25088/ComplexSystems.35.3.203

conditions, a dense set of unstable periodic orbits and an absolutely continuous invariant measure. Since the appearance of an influential survey in 1976 [1], it has served as the standard entry point to nonlinear dynamics in ecology, physics, economics and engineering [2–4].

1.1 Motivation

Nothing in the mathematics here is new, and no claim to the contrary is made. The motivation is instead a practical difficulty that anyone who has taught this material will recognize. A reader who wants to understand the whole picture, not merely the bifurcation diagram as a picture but the reasons it looks as it does, the values of the numbers in it and the means of computing them correctly, must currently assemble that understanding from at least four kinds of sources:

- textbooks that treat local stability carefully but stop short of symbolic dynamics [2]
- texts that develop conjugacy and shift spaces rigorously but assume the reader already accepts the numerical picture [4, 5]
- the original renormalization literature, which is not accessible to a first-year graduate student [6]
- informal code, in lecture notes, weblog posts and repositories, which supplies the pictures but in which errors can remain invisible, because the output still resembles the familiar diagram

The last of these deserves emphasis, because it is the specific gap this paper addresses. A bifurcation diagram computed with too short a transient, a Lyapunov exponent evaluated at the wrong point of an orbit or a table of period-four points that silently contains an unstable fixed point will all produce plausible output. Errors of this kind are easy to make in a compressed treatment and are detectable only when a closed form is available for comparison. Section 9 therefore treats numerical practice as a subject in its own right, and every numerical table in this paper is subjected to an independent consistency check, an exact benchmark or a higher-precision computation.

1.2 Contribution

The contribution is stated precisely here, since it is expository and numerical rather than mathematical.

1. A single self-contained development running from linear stability to a complete proof of Devaney chaos at $\mu = 4$ (Sections 3 through 8), with every step proved rather than asserted.
2. Careful treatment of two points that are easy to get wrong in a compressed account: the non-hyperbolic parameter $\mu = 3$ (Proposition 1) and the distinction between a genuine cycle of period 2^n and the unstable lower-period orbits that coexist with it (Section 4.3).

3. Period-doubling parameters computed to 10 significant figures by a two-variable Newton method, together with an explicit demonstration (Section 5.3) that thresholds given to only four decimal places are structurally incapable of exhibiting convergence to the Feigenbaum constant, a point that can mislead a reader attempting to reproduce it.
4. A reproducibility protocol and reference implementation (Section 9 and the Appendix), with the principal numerical results checked against exact formulas, multiplier criteria or independent higher-precision computations.

Section 2 fixes notation and establishes invariance of the unit interval. Section 3 treats fixed points and their bifurcations. Section 4 derives the period-two orbit in closed form, together with its exact stability window. Section 5 computes the cascade and the Feigenbaum scaling. Section 6 develops Lyapunov exponents, including the exact value at $\mu = 4$. Section 7 proves the conjugacy with the tent map, and Section 8 uses it to prove chaos. Section 9 documents the numerical methods, Section 10 discusses the figures and Section 11 the limitations.

2. Preliminaries

Definition 1. For $x_0 \in [0, 1]$, the orbit of x_0 is the sequence $(x_n)_{n\geq 0}$ with $x_{n+1} = f_\mu(x_n)$. Write f_μ^n for the n-fold composite, so that $x_n = f_\mu^n(x_0)$. Throughout, a superscript on a map denotes composition and never a power.

Definition 2. A point $\overline{x}$ is periodic of period p if $f_\mu^p(\overline{x}) = \overline{x}$ and $f_\mu^k(\overline{x}) \neq \overline{x}$ for $0 < k < p$. The multiplier of the cycle $\{\overline{x}_0, \ldots, \overline{x}_{p-1}\}$ is

$$m = \left(f_\mu^p\right)'(\overline{x}_0) = \prod_{i=0}^{p-1} f_\mu'(\overline{x}_i), \tag{2}$$

which by the chain rule does not depend on the point chosen on the cycle. The cycle is attracting if $|m| < 1$, repelling if $|m| > 1$ and non-hyperbolic if $|m| = 1$.

That the multiplier is a property of the cycle rather than of a point is the single most useful piece of bookkeeping in what follows, since it permits stability to be tested at whichever point of the cycle is most convenient.

Lemma 1. For $0 \leq \mu \leq 4$, $f_\mu([0, 1]) \subseteq [0, 1]$.

https://doi.org/10.25088/ComplexSystems.35.3.203

Proof. The map f_μ is a downward parabola with roots at 0 and 1, so $f_\mu \geq 0$ on [0, 1]. Its maximum on [0, 1] occurs at the critical point $c = 1/2$, where $f_\mu(1/2) = \mu/4 \leq 1$ precisely when $\mu \leq 4$. □

Lemma 1 is the reason the parameter range stops at four. For $\mu > 4$, a neighborhood of $1/2$ escapes the unit interval and the bounded dynamics takes place instead on a Cantor set, a genuinely different situation that is not treated here.

Two further quantities are used repeatedly:

$$f'_\mu(x) = \mu(1 - 2x), \quad f''_\mu(x) = -2\mu, \quad f'''_\mu(x) = 0. \tag{3}$$

3. Fixed Points and Local Bifurcations

3.1 Location

Fixed points solve $f_\mu(x^*) = x^*$, that is, $x^*(\mu(1 - x^*) - 1) = 0$, giving

$$x_0^* = 0, \quad x_+^* = \frac{\mu - 1}{\mu} \quad (\mu \neq 0). \tag{4}$$

The second lies in the unit interval only for $\mu \geq 1$; for $\mu < 1$ it is negative and dynamically irrelevant.

3.2 Linear Stability

Theorem 1. For the map given in equation (1): (a) the fixed point $x_0^* = 0$ has multiplier μ and is attracting for $0 \leq \mu < 1$ and repelling for $\mu > 1$; (b) the fixed point $x_+^* = (\mu - 1)/\mu$ has multiplier $2 - \mu$ and is attracting for $1 < \mu < 3$ and repelling for $\mu > 3$.

Proof. From equation (3), $f'_\mu(0) = \mu$, which gives (a). For (b),

$$f'_\mu\left(\frac{\mu - 1}{\mu}\right) = \mu\left(1 - \frac{2(\mu - 1)}{\mu}\right) = \mu - 2(\mu - 1) = 2 - \mu,$$

and $|2 - \mu| < 1$ holds if and only if $1 < \mu < 3$. Hyperbolicity in each case gives local attraction or repulsion by the linearization theorem for one-dimensional maps [3, Chapter 1]. □

Remark 1. At $\mu = 2$ the multiplier $2 - \mu$ vanishes, so $x_+^* = 1/2$ coincides with the critical point and convergence is quadratic rather than geometric. This is the first member of the superstable family used in Section 5.4. It also explains why the Lyapunov exponent at $\mu = 2$ is $-\infty$, although a double-precision estimate of it settles instead at a floating-point floor, as discussed in Section 6.

3.3 The Transcritical Bifurcation

At $\mu = 1$ the two fixed points collide, since $x_+^* = 0 = x_0^*$, and the multiplier of each equals one. They exchange stability as μ crosses one, in

a transcritical bifurcation. Ecologically this is the extinction threshold: for $\mu < 1$ every orbit in the unit interval converges to zero, and the population dies out regardless of its initial size.

3.4 The Marginal Case

The parameter $\mu = 3$ is routinely described in expository treatments as the point at which the fixed point becomes unstable and a period-two orbit appears. Strictly, both halves of that statement are false at $\mu = 3$; they become true only for $\mu > 3$. Since this is exactly the kind of detail a careful reader will check, the correct result is stated in full.

Proposition 1. At $\mu = 3$ the fixed point $x_+^* = 2/3$ is non-hyperbolic, with multiplier -1. It is nevertheless attracting: every $x_0 \in (0, 1)$ satisfies $f_3^n(x_0) \to 2/3$. Moreover f_3 possesses no period-two orbit.

Proof. The multiplier is $2 - \mu = -1$, so linearization is inconclusive, and the second iterate must be examined. At $\mu = 3$ it factors completely: expanding $f_3^2(x) - x$ and collecting terms gives the identity

$$f_3^2(x) - x = -x(3x - 2)^3, \tag{5}$$

which drives the whole proof. Two consequences are immediate. First, the only solutions of $f_3^2(x) = x$ are $x = 0$ and $x = 2/3$, both of them fixed points of f_3 itself, so f_3 has no orbit of at least period two; this is the third claim. Second, on $(0, 1)$ the sign of $f_3^2(x) - x$ is positive for $x < 2/3$ and negative for $x > 2/3$. A companion identity for the map itself, $f_3(x) - x = x(2 - 3x)$, gives $f_3(x) > x$ on $(0, 2/3)$ and $f_3(x) < x$ on $(2/3, 1)$.

Global convergence. Let $x_0 \in (0, 1)$ and put $J = [9/16, 3/4]$. Since $f_3([0, 1]) = [0, 3/4]$, every iterate after the first lies in $(0, 3/4]$. The interval J is invariant: it lies in $[1/2, 1]$, where f_3 is decreasing, and $f_3(3/4) = 9/16$ while $f_3(9/16) = 189/256 < 3/4$, so $f_3(J) = [9/16, 189/256] \subseteq J$.

Suppose the orbit never enters J. Then $x_n < 9/16 < 2/3$ for every $n \geq 1$, so by the companion identity, the sequence $(x_n)_{n \geq 1}$ is strictly increasing and bounded above by $9/16$. It therefore converges, and its limit is a fixed point of f_3 lying in $(0, 9/16]$. But the only fixed points are 0 and $2/3$, and neither lies in that interval, a contradiction. The orbit must therefore enter J.

Once the orbit is in J, set $g = f_3^2$. Since f_3 is decreasing on J and maps J into itself, g is increasing on J. By equation (5) its only fixed point there is $2/3$, with $g(x) > x$ below it and $g(x) < x$ above it, so an increasing g leaves each of $[9/16, 2/3]$ and $[2/3, 3/4]$ invariant. The g-orbit is thus monotone and bounded, hence convergent, and its limit is a fixed point of g in J, namely $2/3$. Let x_N be the first iterate lying in J. Since J is invariant, x_{N+1} lies in J as well, and applying the

https://doi.org/10.25088/ComplexSystems.35.3.203

preceding argument to each of x_N and x_{N+1} shows that the two parity subsequences converge to $2/3$ from index N onward. Hence (x_n) converges to $2/3$.

Rate. Setting $x = 2/3 + u$ in equation (5) and using $3x - 2 = 3u$ gives exactly

$$f_3^2\left(\frac{2}{3} + u\right) = \frac{2}{3} + u - 18u^3 - 27u^4.$$

The cubic coefficient is negative and there is no quadratic term, so the recursion $u \mapsto u - 18u^3$ has the algebraic decay $|u| \sim (36k)^{-1/2}$ after k steps of g, that is,

$$\left|x_n - \frac{2}{3}\right| \sim (18n)^{-1/2} \tag{6}$$

after n steps of f_3, rather than the geometric decay of the hyperbolic case. □

Remark 2. Attraction also follows from general theory without the factorization. The Schwarzian derivative

$$Sf_\mu(x) = \frac{f_\mu'''}{f_\mu'} - \frac{3}{2}\left(\frac{f_\mu''}{f_\mu'}\right)^2 = -\frac{6}{(1-2x)^2}$$

is negative wherever it is defined, that is, at every $x \neq 1/2$, and a non-hyperbolic fixed point with multiplier -1 belonging to a map with negative Schwarzian derivative is attracting [7]. The elementary argument in the proof was given in preference because it yields the global basin and the convergence rate at the same time.

Numerically, iterating from $x_0 = 0.1$ at $\mu = 3$ gives $|x_n - 2/3| \approx 2.36 \times 10^{-4}$ after 10^6 steps, against the 2.357×10^{-4} predicted by equation (6). This confirms attraction, and it is the origin of a common numerical trap: at $\mu = 3$ a run of a few hundred iterations has not converged, and when plotted it is easily mistaken for a small-amplitude oscillation.

4. The Period-Two Orbit

4.1 Closed Form

Expanding $f_\mu^2(x) = x$ and factoring out the two known fixed points leaves the quadratic $\mu^2 x^2 - \mu(\mu+1)x + (\mu+1) = 0$, whose discriminant is $\mu^2(\mu+1)(\mu-3)$. This is negative for $\mu < 3$ and vanishes at $\mu = 3$, in agreement with Proposition 1, and it is positive for $\mu > 3$, which gives the following.

Theorem 2. For $\mu > 3$, the map f_μ has a unique period-two orbit $\{p_-, p_+\}$ with

$$p_\pm = \frac{(\mu + 1) \pm \sqrt{(\mu + 1)(\mu - 3)}}{2\mu}. \tag{7}$$

Its multiplier is

$$m_2(\mu) = f'_\mu(p_-)f'_\mu(p_+) = 4 + 2\mu - \mu^2, \tag{8}$$

and the orbit is attracting precisely for

$$3 < \mu < 1 + \sqrt{6} = 3.449489742\ldots. \tag{9}$$

Proof. Equation (7) is the quadratic formula. For the multiplier, note that $p_- + p_+ = (\mu + 1)/\mu$ and $p_-p_+ = (\mu + 1)/\mu^2$ by the relations between roots and coefficients. Then

$$m_2 = \mu^2(1 - 2p_-)(1 - 2p_+) = \mu^2(1 - 2(p_- + p_+) + 4p_-p_+),$$

and substituting the symmetric functions gives $m_2 = \mu^2 - 2\mu(\mu + 1) + 4(\mu + 1) = 4 + 2\mu - \mu^2$. Solving $-1 < 4 + 2\mu - \mu^2 < 1$ for $\mu > 3$, the right inequality holds for every $\mu > 3$, while $4 + 2\mu - \mu^2 > -1$ gives $\mu^2 - 2\mu - 5 < 0$, that is, $\mu < 1 + \sqrt{6}$. □

Remark 3. Note that $m_2(3) = +1$, not -1. The period-two orbit is born tangentially from the fixed point as μ crosses three, inheriting the multiplier through a period-doubling bifurcation of the fixed point, whose own multiplier is -1 there. It then loses stability at $\mu = 1 + \sqrt{6}$, where $m_2 = -1$, giving birth to the period-four orbit. Each subsequent doubling repeats this pattern, and it is this self-similar repetition that renormalization theory explains.

4.2 Numerical Confirmation

Table 1 tracks convergence to the period-two orbit at $\mu = 3.22$ and $\mu = 3.3$. Because consecutive iterates of f_μ alternate between the two branches of the cycle, the natural object to tabulate is the orbit of the second iterate f_μ^2, whose iterates settle onto one branch of the two-cycle, possibly after an initial overshoot. The entries are therefore $x_{2k} = f_\mu^{2k}(x_0)$; the odd-indexed iterates converge to the other branch.

The two rows given for each μ illustrate a point worth making explicitly to students. The rows starting at $x_0 = 0.2$ converge to four decimal places within four steps of f_μ^2, whereas those starting at $x_0 = 0.1$ are still visibly drifting at x_8. Both converge to the same cycle. The orbit from $x_0 = 0.1$ approaches $p_- = 0.505662$ from above, having been carried by two steps of f_μ to $x_2 = 0.6627$, close to

the repelling fixed point $x_+^* = 0.6894$; the transient is far longer because the orbit must escape the neighborhood of that repelling point before settling. Escape from a repelling fixed point with multiplier $2 - \mu$ takes roughly $\ln(\varepsilon^{-1}) / \ln|2 - \mu|$ steps, which at $\mu = 3.22$ is slow. This is precisely why the transient discarding described in Section 9 is not a formality.

μ	x_0	x_2	x_4	x_6	x_8	Limit $p_\pm$
3.22	0.1	0.6627	0.6495	0.6302	0.6031	0.505662
3.22	0.2	0.8043	0.8048	0.8049	0.8049	0.804897
3.30	0.1	0.6890	0.6835	0.6740	0.6577	0.479427
3.30	0.2	0.8224	0.8239	0.8235	0.8236	0.823603

Table 1. Convergence to the period-two orbit. Entries are iterates of the second composite $x_{2k} = f_\mu^{2k}(x_0)$, since consecutive iterates of f_μ itself alternate between the two branches and converge to nothing. The final column gives the closed-form limit from equation (7), which agrees to the digits shown.

4.3 Period Four and the Coexistence of Unstable Orbits

Beyond $\mu = 1 + \sqrt{6}$, the period-two orbit becomes repelling and a period-four orbit appears. It is essential to recognize that the older orbits do not disappear. Throughout the attracting period-four window, the equation $f_\mu^4(x) = x$ has eight real solutions in the unit interval: the two fixed points 0 and x_+^*, the two points of the repelling period-two orbit and the four points of the attracting period-four orbit.

This coexistence is the source of a specific and easily made error. A numerical routine that solves $f_\mu^4(x) = x$ or that reads points off a plot of f_μ^4 against the diagonal returns all eight of these together. Unless the multiplier of equation (2) is computed for each, the unstable fixed point and the unstable two-cycle points are indistinguishable in the output from the genuine four-cycle. Selecting the wrong four produces a table that is numerically accurate and dynamically meaningless.

Table 2 therefore reports the attracting cycle only, identified by iterating past a long transient and verified by the criterion $|m| < 1$. The cycle points are listed in increasing order together with the cycle multiplier.

The multiplier column makes the mechanism visible in a way the orbit values alone do not. The multiplier enters the window near $+1$ at $\mu = 3.45$, just after the four-cycle is born from the two-cycle, decreases monotonically through zero near $\mu \approx 3.4986$, which is the

superstable parameter at which the cycle contains the critical point and convergence is fastest, and reaches -1 near $\mu \approx 3.5441$, where the four-cycle in turn gives birth to the eight-cycle. Every window in the cascade has this same internal structure, traversed ever more quickly as the period grows.

μ	p	$\overline{x}_{(1)}$	$\overline{x}_{(2)}$	$\overline{x}_{(3)}$	$\overline{x}_{(4)}$	m
3.44	2	0.442193	—	—	0.848505	−0.9536
3.45	4	0.433992	0.445968	0.847468	0.852428	+0.9900
3.46	4	0.413234	0.467486	0.838952	0.861342	+0.7923
3.47	4	0.402914	0.478561	0.834793	0.865905	+0.5915
3.48	4	0.395064	0.487159	0.831680	0.869426	+0.3874
3.49	4	0.388521	0.494446	0.829127	0.872392	+0.1801
3.50	4	0.382820	0.500884	0.826941	0.874997	−0.0305
3.51	4	0.377722	0.506713	0.825019	0.877342	−0.2445
3.52	4	0.373084	0.512076	0.823301	0.879487	−0.4619
3.53	4	0.368812	0.517068	0.821748	0.881472	−0.6828
3.54	4	0.364840	0.521754	0.820331	0.883325	−0.9072
3.55	8	See caption				+0.4497

Table 2. Attracting cycles, verified by the multiplier test. Cycles were obtained after a transient of 4×10^5 iterations and confirmed by the criterion of equation (2). The parameter $\mu = 3.44$ still carries a two-cycle, lying below $1 + \sqrt{6} = 3.449490$, and $\mu = 3.55$ already carries an eight-cycle, namely 0.354800, 0.370326, 0.506031, 0.540475, 0.812656, 0.827805, 0.881684 and 0.887371. Only the intermediate rows are genuinely of period four.

For contrast, Table 3 lists the fixed point x_+^* over the same range. These values are correct, but they describe a repelling object throughout, the multiplier $2 - \mu$ having modulus between 1.44 and 1.55 there. No orbit converges to them, and they should not be confused with the attracting cycles of Table 2.

μ	3.44	3.46	3.48	3.50	3.52	3.55
x_+^*	0.7093	0.7110	0.7126	0.7143	0.7159	0.7183
$2 - \mu$	−1.44	−1.46	−1.48	−1.50	−1.52	−1.55

Table 3. The fixed point and its multiplier over the period-four window. The fixed point $x_+^* = (\mu - 1)/\mu$ persists throughout this range but is repelling, since $|2 - \mu| > 1$. It is not part of any attracting cycle listed in Table 2 .

https://doi.org/10.25088/ComplexSystems.35.3.203

5. The Cascade and Feigenbaum Scaling

5.1 Definition of the Thresholds

Let μ_n denote the parameter at which the attracting cycle of period 2^{n-1} on the principal cascade loses stability and the cycle of period 2^n is born. It is located by solving

$$f_\mu^{2^{n-1}}(x) = x \quad \text{and} \quad \left(f_\mu^{2^{n-1}}\right)'(x) = -1 \tag{10}$$

for the pair (μ, x). The system does not characterize μ_n by itself: other periodic branches, such as those inside the period-three window, produce further solutions. What selects the principal branch is the initialization of the Newton iteration described next, which starts from a point known to lie on the cycle in question. On that branch, the values $\mu_1 = 3$ and $\mu_2 = 1 + \sqrt{6}$ are known exactly from Theorems 1 and 2, and they serve as checks on the solver. From $n = 3$ onward, no closed form is available.

5.2 Computing the Thresholds Accurately

The system in equation (10) consists of two equations in the two unknowns μ and x, and it is solved here by the Newton method in extended precision, using the recursion

$$\left(f_\mu^N\right)'(x) = \prod_{i=0}^{N-1} \mu(1 - 2x_i) \tag{11}$$

to evaluate the derivative without symbolic differentiation. This is substantially more accurate than the usual approach of scanning μ and detecting a change of period, whose resolution is limited by the period-detection tolerance. Results appear in Table 4.

n	μ_n	$\mu_n - \mu_{n-1}$	$\mu_{n+1} - \mu_n$	δ_n
1	3.000000000	—	0.4494897	—
2	3.449489743	0.4494897	0.0946006	4.75145
3	3.544090360	0.0946006	0.0203169	4.65625
4	3.564407266	0.0203169	0.0043522	4.66824
5	3.568759420	0.0043522	—	—

Table 4. Period-doubling thresholds and the associated ratios. Thresholds were obtained from a two-variable Newton solve of equation (10) at 50-digit precision, and the ratios are $\delta_n = (\mu_n - \mu_{n-1})/(\mu_{n+1} - \mu_n)$. The first two thresholds agree with the exact values 3 and $1 + \sqrt{6}$.

5.3 Why Four Decimal Places Are Not Enough

The ratios in Table 4 approach the Feigenbaum constant $\delta = 4.669201609\ldots$ [6] from a sequence that is not monotone, and

the approach is visibly slow. The reason is worth setting out, since it is easy to mistake for a defect in the computation.

Consider forming the ratios from thresholds rounded to four decimal places, as is commonly done. By $n = 4$ the numerator $\mu_4 - \mu_3$ is approximately 0.0203, and the denominator $\mu_5 - \mu_4$ is approximately 0.00435. A rounding error of 5×10^{-5} in each threshold propagates to a relative error of order $10^{-4} / 0.00435$, roughly two percent, in δ_4, and the situation degrades by a factor of δ at each subsequent level. Within a further level or two, the denominator falls below the rounding error itself and the computed ratio becomes meaningless. Already at this precision, rounded values such as 3.5440, 3.5644 and 3.5688 produce ratios between 4.63 and 4.89 that neither converge nor bracket the true constant.

The remedy is not more iterations but more digits. The differences $\mu_{n+1} - \mu_n$ shrink geometrically by a factor of about 4.67, so extracting k correct digits of δ at level n requires roughly $k + n\log_{10}\delta$ digits in μ_n. This is why Table 4 was computed at 50-digit precision.

5.4 Superstable Parameters

An independent and better-conditioned route to δ uses the *superstable* parameters s_n, at which the critical point lies on the cycle of period 2^n:

$$f_{s_n}^{2^n}\left(\frac{1}{2}\right) = \frac{1}{2}. \tag{12}$$

Equation (12) alone does not determine s_n, because every earlier superstable parameter also satisfies it: if the critical point lies on a cycle of period 2^k with $k < n$, it lies on a cycle of period dividing 2^n as well, so $s_0 = 2$ is a root of the equation at every level. The sequence intended here is the one on the principal period-doubling cascade. Accordingly, set $s_0 = 2$ and, for $n \geq 1$, let s_n be the root of equation (12) lying in (μ_n, μ_{n+1}); that root is unique, and the interlacing $\mu_n < s_n < \mu_{n+1}$ then holds by construction for $n \geq 1$.

So defined, equation (12) is a single equation in a single unknown with a transversal root, which makes it far better conditioned numerically than equation (10). The superstable parameters obey the same asymptotic scaling as the thresholds. Table 5 shows the resulting ratios converging more cleanly toward δ.

Both sequences accumulate at

$$\mu_\infty = 3.569945672\ldots, \tag{13}$$

the accumulation point of the principal period-doubling cascade. It is not a boundary between periodic and chaotic behavior: attracting cycles occur at parameters well above it, in the periodic windows,

https://doi.org/10.25088/ComplexSystems.35.3.203

most prominently the period-three window beginning at $\mu = 1 + \sqrt{8} = 3.828427\ldots$, whose existence forces cycles of every period [8]. What distinguishes μ_∞ is that the principal chaotic bands appear immediately above it.

n	s_n	$(s_n - s_{n-1})/(s_{n+1} - s_n)$
0	2.000000000	—
1	3.236067977	4.708943
2	3.498561699	4.680771
3	3.554640863	4.662960
4	3.566667380	4.668404
5	3.569243532	4.668954
6	3.569795294	—

Table 5. Superstable parameters and their ratios. Parameters were obtained from equation (12), and the ratios converge to the same constant $\delta = 4.669201609\ldots$ as those of Table 4, but more smoothly. The first two entries agree with the exact values 2 and $1 + \sqrt{5}$, providing a check on the solver.

The universality of δ, meaning that the same constant governs the cascade throughout a broad class of smooth unimodal maps with a quadratic critical point, under the usual hypotheses, is the deepest fact in this circle of ideas and the reason the logistic map is worth studying at all rather than as a mere curiosity. It is a fixed-point property of a renormalization operator acting on a space of maps, and lies beyond the present scope; see [5, 6].

6. Lyapunov Exponents

6.1 Definition

Definition 3. The Lyapunov exponent of the orbit of x_0 is

$$\lambda(x_0) = \lim_{n\to\infty} \frac{1}{n} \sum_{i=0}^{n-1} \ln\left|f'_\mu(x_i)\right|, \tag{14}$$

when the limit exists.

The interpretation is direct. A perturbation δ_0 of the initial condition is amplified after n steps by $\left|(f_\mu^n)'(x_0)\right| = \prod_i \left|f'_\mu(x_i)\right|$, so that $|\delta_n| \approx |\delta_0| e^{\lambda n}$. A positive exponent means exponential separation of initially nearby orbits, which is sensitive dependence, while a negative

exponent means contraction onto an attractor. When $\lambda > 0$, the quantity $1/\lambda$ has units of iterations and is the e-folding time of a perturbation; the horizon over which prediction remains useful is a multiple of it, depending logarithmically on the initial uncertainty and on the error one is prepared to tolerate.

By the Birkhoff ergodic theorem, if f_μ admits an ergodic invariant measure ν with $\ln|f'_\mu|$ integrable, then λ is independent of x_0 for ν-almost every x_0 and equals the integral of $\ln|f'_\mu|$ against ν. This is why a single trajectory suffices in practice.

6.2 Closed Forms on Periodic Attractors

When the attractor is a cycle of period p with multiplier m, the orbit visits each cycle point equally often and equation (14) collapses to

$$\lambda = \frac{1}{p} \ln|m|. \tag{15}$$

This provides exact values against which any implementation can be tested. On the stable fixed point, $\lambda = \ln|2 - \mu|$; on the stable two-cycle, $\lambda = \frac{1}{2}\ln|4 + 2\mu - \mu^2|$. At every superstable parameter, the multiplier vanishes and $\lambda = -\infty$, which is the correct answer and the reason numerical estimates plunge sharply near those parameters rather than tracking a smooth curve.

6.3 The Exact Value at Full Development

Theorem 3. The map f_4 preserves the probability measure with density

$$\rho(x) = \frac{1}{\pi\sqrt{x(1-x)}}, \tag{16}$$

and with respect to that measure $\lambda = \ln 2$.

Proof. Invariance of the density in equation (16) follows from the conjugacy of Theorem 4: the map $h(x) = \sin^2(\pi x/2)$ pushes the Lebesgue measure on the unit interval, which the tent map preserves, forward to the measure with density ρ. For the exponent, substitute $x = \sin^2(\pi t/2)$ in

$$\lambda = \int_0^1 \ln|4 - 8x|\rho(x)dx.$$

Under this substitution, $|f'_4(x)| = |4 - 8x| = 4|\cos(\pi t)|$, and

$$\rho(x)dx = \frac{2}{\pi\sin(\pi t)} \cdot \frac{\pi}{2}\sin(\pi t)dt = dt,$$

https://doi.org/10.25088/ComplexSystems.35.3.203

so the integral becomes

$$\lambda = \int_0^1 \ln|4\cos(\pi t)|dt = \ln 4 + \int_0^1 \ln|\cos(\pi t)|dt.$$

The classical log-cosine integral evaluates to $-\ln 2$, whence $\lambda = 2\ln 2 - \ln 2 = \ln 2$. □

Thus $\lambda = \ln 2 \approx 0.6931$: at $\mu = 4$ each iteration destroys on average one bit of information about the initial condition. Since double precision carries about 53 bits, this sets a predictability horizon of some tens of iterations for machine-scale initial uncertainty, a point taken up again in Section 9.

6.4 Numerical Values

Table 6 compares computed exponents with closed forms where these are available.

μ	Computed λ	Exact	Attractor
2.0000	−36.04	$-\infty$	superstable fixed point
2.5000	−0.69315	−0.69315	fixed point
3.2000	−0.91629	−0.91629	two-cycle
3.4000	−0.13722	−0.13722	two-cycle
3.5000	−0.87251	—	four-cycle
3.5500	−0.09989	—	eight-cycle
3.5699	−0.00379	—	near accumulation
3.5700	+0.01101	—	chaotic
3.6000	+0.18357	—	chaotic
3.7000	+0.35501	—	chaotic
3.8300	−0.36967	—	period-three window
3.9000	+0.49626	—	chaotic
4.0000	+0.69315	+0.69315	chaotic

Table 6. Computed Lyapunov exponents against closed forms. Exponents were computed from equation (14) with 2×10^6 iterations after a transient of 10^5. Exact values come from equation (15) and Theorem 3. At $\mu = 2$ the exact value is $-\infty$, and the finite figure shown is a floating-point floor rather than a truncation artifact: in IEEE double precision, the orbit stalls at a machine neighbor of $1/2$, where $|1 - 2x| \approx 1.1\times10^{-16}$, so $|f_2'|$ is pinned near machine precision, and the estimate settles at −36.04 irrespective of the iteration count.

Two entries deserve comment. The row at $\mu = 3.83$ has a negative exponent despite lying deep in what is loosely called the chaotic region, because it falls inside the period-three window, where the attractor is again a stable cycle. Chaos is not an interval of parameters but a set riddled with such windows, and a coarse grid in μ will

step over them entirely. The rows at 3.5699 and 3.5700 bracket the accumulation point of equation (13) and show the exponent changing sign in its vicinity. This is not the first zero of λ: the exponent vanishes at every threshold μ_n, including $\mu_1 = 3$, since the multiplier of the attracting cycle has modulus one there. What is specific to μ_∞ is that immediately above it, the principal chaotic bands carry a positive exponent.

7. Conjugacy with the Tent Map

7.1 Statement

Define the tent map T on the unit interval by

$$T(x) = \begin{cases} 2x, & x < 1/2, \\ 2(1-x), & x \geq 1/2. \end{cases} \tag{17}$$

Definition 4. Maps F on X and G on Y are topologically conjugate if there is a homeomorphism h from X to Y with $h \circ F = G \circ h$.

Theorem 4. Let $h(x) = \sin^2(\pi x/2)$. Then h is a homeomorphism of the unit interval onto itself and

$$h \circ T = f_4 \circ h. \tag{18}$$

Proof. The map h is continuous, $h(0) = 0$, $h(1) = 1$ and $h'(x) = (\pi/2)\sin(\pi x) > 0$ on the open interval, so h is a strictly increasing continuous bijection of a compact interval and hence a homeomorphism.

For the intertwining relation, compute the right-hand side using the double-angle identity:

$$f_4(h(x)) = 4\sin^2\frac{\pi x}{2}\left(1 - \sin^2\frac{\pi x}{2}\right) = 4\sin^2\frac{\pi x}{2}\cos^2\frac{\pi x}{2} = \sin^2(\pi x).$$

For the left-hand side, check the two branches of equation (17). If $x < 1/2$, then $h(T(x)) = h(2x) = \sin^2(\pi x)$. If $x \geq 1/2$, then

$$h(T(x)) = h(2 - 2x) = \sin^2(\pi(1-x)) = \sin^2(\pi x),$$

since $\sin(\pi - \theta) = \sin\theta$. Both branches agree with $f_4(h(x))$, establishing equation (18). □

Corollary 1. The map h carries orbits of T bijectively onto orbits of f_4, preserving period, and maps the set of points of period p for T onto the set of points of period p for f_4.

Proof. Iterating equation (18) gives $h \circ T^n = f_4^n \circ h$ for every n, so $T^p(x) = x$ if and only if $f_4^p(h(x)) = h(x)$. □

https://doi.org/10.25088/ComplexSystems.35.3.203

7.2 The Reach of Conjugacy

Conjugacy is a strong equivalence, and its reach is worth stating explicitly, because expository accounts sometimes overclaim. Since h is a homeomorphism, it preserves every purely topological property: periods and the structure of the set of periodic points, topological transitivity, density of periodic orbits, minimality and topological entropy. It also carries invariant measures to invariant measures by pushforward, which is how Theorem 3 was obtained.

It does not preserve metric quantities in general. The map h is smooth on the closed interval, but its derivative vanishes at the endpoints, since $h'(0) = h'(1) = 0$, so it is not a diffeomorphism whose derivative is bounded away from zero; equivalently, the derivative of h^{-1} is unbounded near the endpoints. Distances, and quantities defined through them, therefore need not correspond. For this reason, the exponent in Theorem 3 is not obtained by appealing to conjugacy as a general principle, but from the explicit integral against the invariant density; the role of the conjugacy there is only to identify that density as the pushforward of the Lebesgue measure.

7.3 The Tent Map and the Binary Shift

The tent map is convenient because it is piecewise linear, with derivative of modulus two at every point except the turning point $x = 1/2$, where it is not differentiable. Since that is a single point, and hence of Lebesgue measure zero, the entropy and the Lyapunov exponent are immediate. It is in turn semiconjugate to the doubling map $x \mapsto 2x$ modulo one, whose action in binary is simply to delete the leading digit. This chain, running from the binary shift through the tent map to f_4, is what permits combinatorial information about sequences of symbols to be transferred into analytic statements about the logistic map. That transfer is made explicit next.

8. Symbolic Dynamics and a Proof of Chaos

8.1 Itineraries

Partition the unit interval as $I_0 = [0, 1/2)$ and $I_1 = [1/2, 1]$, and let $\Sigma_2 = \{0, 1\}^{\mathbb{N}}$ carry the product topology, the metric

$$d(s, t) = \sum_{i \geq 0} \frac{|s_i - t_i|}{2^i}, \tag{19}$$

and the shift map $\sigma(s_0 s_1 s_2 \ldots) = s_1 s_2 s_3 \ldots$.

Definition 5. The itinerary of x in the unit interval under f_4 is the sequence $S(x) = (s_0 s_1 s_2 \ldots)$ with $s_n = j$ whenever $f_4^n(x) \in I_j$.

Theorem 5. The relation $S \circ f_4 = \sigma \circ S$ holds; that is, applying the map advances the itinerary by one symbol.

Proof. The symbol in position n of $S(f_4(x))$ records the location of $f_4^n(f_4(x)) = f_4^{n+1}(x)$, which is the symbol in position $n+1$ of $S(x)$, and hence the symbol in position n of $\sigma(S(x))$. □

Theorem 5 records the compatibility of the itinerary coding with the shift. The proof of Devaney chaos in Section 8.4 proceeds separately through the conjugate tent map via Theorem 4. Away from the countable set of points whose orbit meets the partition boundary, the itinerary determines the orbit uniquely; boundary itineraries require the usual coding convention and are not needed here.

8.2 Two Worked Examples

Example 1. Take $x_0 = 0.3$. The first iterates under f_4 are

$$0.3,\ 0.84,\ 0.5376,\ 0.99434,\ 0.02249,\ 0.08794,\ 0.32084,\ \ldots$$

giving the itinerary

$$S(0.3) = 011100010100110011001011\ldots$$

with no discernible pattern, as expected, since 0.3 is not a periodic point. It is worth stressing that this is the typical case: periodic points are dense but have Lebesgue measure zero, so a randomly chosen initial condition yields an aperiodic itinerary with probability one.

Example 2. The genuine period-two orbit of f_4 is obtained from $f_4^2(x) = x$ after removing the fixed points 0 and 3/4:

$$q = \frac{5 - \sqrt{5}}{8} = 0.3454915\ldots, \quad p = \frac{5 + \sqrt{5}}{8} = 0.9045085\ldots$$

One checks that $f_4(q) = p$ and $f_4(p) = q$. Since $q \in I_0$ and $p \in I_1$, the itinerary is the infinite repetition of 01, which is the period-two point of the shift. This is the orbit whose itinerary alternates; the point 0.3 of Example 1 is not on it and does not have that itinerary.

8.3 Counting Periodic Points and Entropy

Proposition 2. The map f_4 has exactly 2^n points of period dividing n, and its topological entropy is ln2.

Proof. By Theorem 4, it suffices to count for T. The graph of T^n consists of 2^n full linear branches of slope $\pm 2^n$, each crossing the diagonal exactly once, which gives 2^n solutions of $T^n(x) = x$. The entropy ln2 follows either from the growth rate of the number of fixed points of T^n for these piecewise monotone maps, or from the Misiurewicz–Szlenk formula applied to the 2^n laps of T^n. Topological entropy is a conjugacy invariant, so the same holds for f_4. □

That the entropy and the Lyapunov exponent are both ln2 is not a coincidence. It is an instance of the Pesin identity, which for a

https://doi.org/10.25088/ComplexSystems.35.3.203

one-dimensional map with an absolutely continuous invariant measure equates metric entropy with the positive Lyapunov exponent.

8.4 Chaos in the Sense of Devaney

Definition 6. A map F on X is chaotic [4] if (a) the periodic points of F are dense in X; (b) F is topologically transitive, meaning that for all nonempty open sets U and V there is an n with $F^n(U) \bigcap V$ nonempty; and (c) F exhibits sensitive dependence on initial conditions.

Theorem 6. The map f_4 is chaotic on the unit interval.

Proof. Chaos in this sense is preserved by topological conjugacy, so by Theorem 4 it suffices to prove the three properties for T.

For (a), given any interval J in the unit interval, choose n with $2^{-n} < |J|/2$. The map T^n has 2^n branches, each defined on a dyadic interval of length 2^{-n} and mapping it onto the whole unit interval. An interval longer than twice the grid spacing must contain a whole grid cell, so at least one such branch domain D lies inside J. Note that $2^{-n} < |J|$ alone would not suffice, since an interval slightly longer than a cell can straddle two cells without containing either. Since the restriction of T^n to D is a surjective linear map onto the unit interval, $T^n(D) \supseteq D$, and the intermediate value theorem applied to $T^n(x) - x$ yields a fixed point of T^n in D, hence in J.

For (b), with U open, pick n and a branch domain D inside U as above; then $T^n(U) \supseteq T^n(D)$, which is the whole unit interval and so meets every nonempty V.

For (c), any $\varepsilon < 1/4$ is a sensitivity constant. Given x and $\eta > 0$, put $J = (x - \eta, x + \eta) \bigcap [0, 1]$, which is a nondegenerate interval whether x lies in the interior or at an endpoint, and choose n with $2^{-n} < |J|/2$. As in (a), a full branch domain D then lies inside J. Since $T^n(D)$ is the whole unit interval, its image contains points at distance at least $1/2$ from $T^n(x)$, so some y in D satisfies $|T^n(y) - T^n(x)| > \varepsilon$.

Property (c) is in fact implied by (a) and (b) on an infinite metric space [9], but the direct argument is short. □

Remark 4. Theorem 6 justifies calling $\mu = 4$ fully chaotic in a precise sense, and it also corrects a claim that is frequently made loosely. It is not true that every orbit of f_4 is dense in the unit interval, since the periodic orbits, dense as a set, are individually finite. What is true is that a dense orbit exists, that for Lebesgue-almost every initial point $x_0 \in [0, 1]$, the orbit of x_0 is dense and equidistributes with respect to the invariant density in equation (16), and that the set of periodic points is dense. The distinction between almost every orbit and every orbit is exactly the distinction between measure-theoretic and topological statements, and it is a distinction easily lost in an informal account.

9. Numerical Methods and Reproducibility

9.1 Protocol

All computations use IEEE double precision unless noted. The thresholds of Table 4 and the superstable parameters of Table 5 use 50-decimal arithmetic.

Cobweb plots (Figures 1 through 5) show 50 iterations with no transient discarded, since the transient is the object of interest. Figures 7 through 10 are graphs of the maps and their iterates rather than trajectory plots, and no iteration protocol applies to them.

Bifurcation diagrams (Figure 6) sample μ at 2400 equally spaced values across each panel and plot 200 iterates at each. Only the transient differs between panels: 10^3 iterations for panel (a), 3×10^3 for panel (b) and 2×10^3 for panels (c) and (d), the longer values being used where the panel resolves a threshold and convergence is correspondingly slow. Increasing the transient from the 500 used in an earlier version of this work visibly sharpens the branches.

The seed is $x_0 = 0.400001$ rather than the critical point $x_0 = 1/2$. The critical point is exceptional: under f_4 it gives $1/2 \mapsto 1 \mapsto 0$, so a diagram seeded there shows a fixed point at its right-hand edge instead of the chaotic attractor. Any generic seed avoids this.

For the Lyapunov exponent curve of Figure 11, 10^4 transient iterations are discarded and the exponent is averaged over the next 2×10^4 iterations at each parameter value, which is sufficient for the resolution of the plotted curve. The selected values of Table 6 use the more stringent protocol of 10^5 transient iterations followed by 2×10^6 averaging iterations, since those are quoted to five decimal places; applying that protocol at every one of the 2401 grid points of the curve would cost some five billion updates for no visible gain. In both cases, the derivative is evaluated at x_i before the state is updated, in accordance with equation (14). Evaluating after the update merely displaces the finite sum by one term, and the two conventions have the same infinite-time limit wherever it exists.

Cycle identification (Table 2) iterates 4×10^5 times, then searches for the smallest period p in $\{1, 2, 4, \ldots, 32\}$ with $\left|x_{i+p} - x_i\right| < 10^{-12}$ for all i in a window of 10^3 points, and finally verifies that $|m| < 1$ using equation (2).

9.2 The Meaning of a Computed Orbit

Section 6 showed that $\lambda = \ln 2$ at $\mu = 4$, so roughly one bit of information about the initial condition is lost per iteration. Double precision carries about 53 bits, which gives a rough predictability horizon of some tens of iterations for machine-scale initial uncertainty. This is an order-of-magnitude estimate rather than a hard cutoff, since the local

https://doi.org/10.25088/ComplexSystems.35.3.203

rate of separation varies along an orbit and the exponent is only an asymptotic average, but its consequence is not in doubt: a long computed chaotic trajectory is not the orbit of the initial condition it was started from.

It does not follow that the computations are without content, and it is worth being precise about why. The claims made here are statistical, concerning the invariant density, the Lyapunov exponent and the structure of the attractor, rather than claims about where any individual orbit is after a given number of steps. Such quantities are validated here directly, not by an appeal to pointwise accuracy: the computed exponent at $\mu = 4$ agrees with the exact value ln2 of Theorem 3, the exponents on periodic attractors agree with the closed form of equation (15), the cycles are confirmed by the multiplier test rather than by their numerical values, and the thresholds are computed in extended precision and checked against 3 and $1 + \sqrt{6}$.

A reader may be tempted to invoke the shadowing property, which guarantees for a uniformly hyperbolic system that an accurate pseudo-orbit stays close to some true orbit, generally with a different initial condition. That justification is not available here without further work, because f_4 is not uniformly hyperbolic on the unit interval: the derivative vanishes at the critical point $x = 1/2$. The point is made explicitly because it is usually omitted from introductory treatments, which can leave the impression either that the computed numbers are the true orbit or that a shadowing theorem applies without qualification.

9.3 Verification

Each table was checked against an independent computation. Table 1 was checked against the closed form of equation (7), Table 2 against the multiplier criterion and against $1 + \sqrt{6}$ for the location of the period-four threshold, Table 4 against the exact values 3 and $1 + \sqrt{6}$ and against the superstable sequence, Table 5 against the exact values 2 and $1 + \sqrt{5}$, and Table 6 against equation (15) and Theorem 3. Source code is given in the Appendix.

10. Reading the Figures

10.1 Cobweb Plots and the Three Regimes

Figure 1, at $\mu = 2$, shows the superstable case. Both initial conditions reach $x^* = 1/2$ in a handful of steps, and the staircase collapses to a point without spiraling, reflecting the vanishing multiplier.

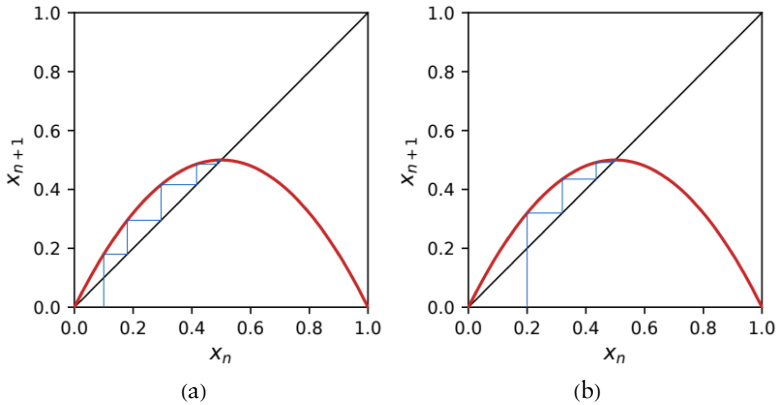


Figure 1. Cobweb plots at $\mu = 2$, the superstable case. Panel (a) uses $x_0 = 0.1$ and panel (b) uses $x_0 = 0.2$. The fixed point $x^* = 1/2$ has multiplier $2 - \mu = 0$, so convergence is quadratic and the staircase collapses without spiraling.

Figure 2, at $\mu = 3$, is the marginal case of Proposition 1. The cobweb spirals inward around $x^* = 2/3$ so slowly that over 50 iterations it appears to close into a loop. It does not; the orbit is converging, at the algebraic rate given in equation (6). This figure is the visual counterpart of Proposition 1, and it illustrates why visual inspection alone is an unreliable guide near non-hyperbolic parameters.

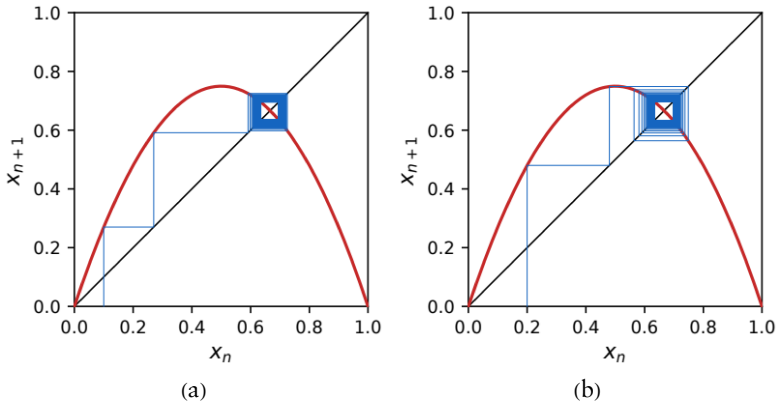


Figure 2. Cobweb plots at $\mu = 3$, the non-hyperbolic case. Panel (a) uses $x_0 = 0.1$ and panel (b) uses $x_0 = 0.2$. The multiplier is -1, so the orbit spirals inward at the algebraic rate of equation (6). Over 50 iterations the loop appears closed, but the fixed point $x^* = 2/3$ is still attracting, and no period-two orbit exists at this parameter, as shown in Proposition 1.

Figures 3 and 4, at $\mu = 3.22$ and $\mu = 3.3$, show the cobweb settling into a rectangle, the signature of a two-cycle, whose corners are

the points $p_{\pm}$ of equation (7). The rectangle is visibly larger at $\mu = 3.3$ than at $\mu = 3.22$, consistent with the separation

$$p_+ - p_- = \frac{\sqrt{(\mu+1)(\mu-3)}}{\mu}, \tag{20}$$

which grows like the square root of $\mu - 3$: the square-root law characteristic of a period-doubling bifurcation.

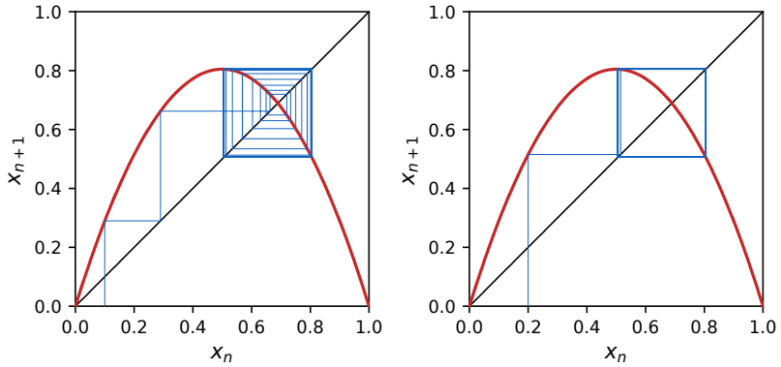


Figure 3. Cobweb plots at $\mu = 3.22$, showing a two-cycle. Panel (a) uses $x_0 = 0.1$ and panel (b) uses $x_0 = 0.2$. The orbit settles onto the rectangle whose corners are the period-two points 0.505662 and 0.804897 from equation (7). Panel (a) shows a longer transient because the second iterate, $x_2 \approx 0.6627$, lies near the repelling fixed point at 0.6894.

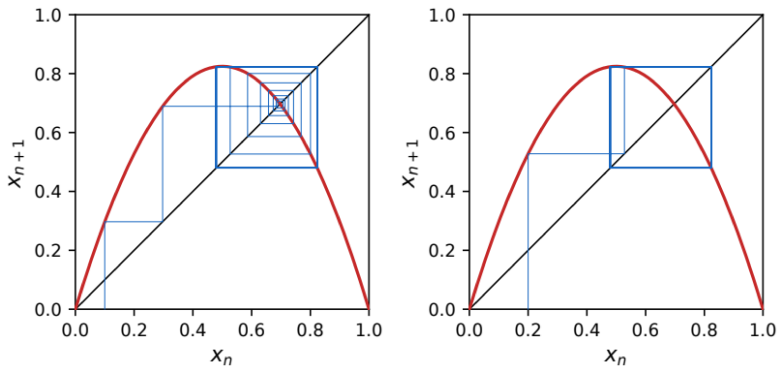


Figure 4. Cobweb plots at $\mu = 3.3$, with period-two points 0.479427 and 0.823603. Panel (a) uses $x_0 = 0.1$ and panel (b) uses $x_0 = 0.2$. Comparison with Figure 3 shows the rectangle widening as the square root of $\mu - 3$, the square-root law of the period-doubling bifurcation.

Figure 5, at $\mu = 4$, shows no such structure: the cobweb spreads broadly through the unit square. The concentration of visited points near the endpoints, apparent on close inspection, is the invariant density of equation (16), which has integrable singularities there. Readers often expect a chaotic orbit to visit the interval uniformly. It does not, and Theorem 3 says exactly how it fails to.

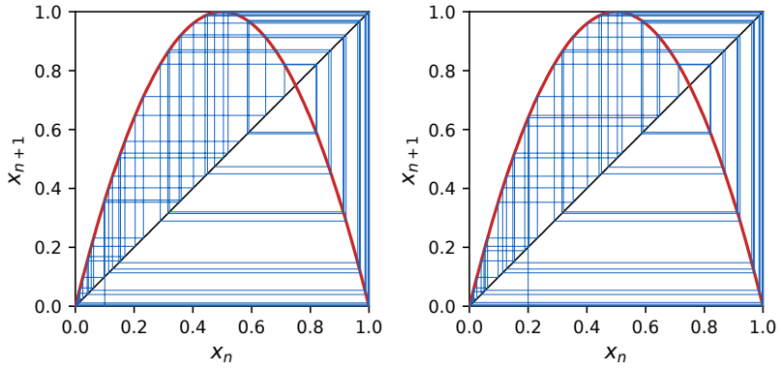


Figure 5. Cobweb plots at $\mu = 4$, the fully developed case. Panel (a) uses $x_0 = 0.1$ and panel (b) uses $x_0 = 0.2$. Iterates spread broadly through the unit square, with visits concentrated near the endpoints in accordance with the invariant density of equation (16).

10.2 Bifurcation Diagrams

Figure 6 covers the cascade in four panels. Panel (a) spans μ from 2.8 to 4 and shows the full cascade, with successive doublings occurring at the thresholds of Table 4, and spacings shrinking by the factor $\delta \approx 4.669$. This geometric compression is what makes the individual bifurcations indistinguishable to the naked eye beyond about the fifth, and it is why the magnified views in the remaining panels are needed.

Panel (b), spanning 3.4 to 3.5, resolves the second doubling at $1 + \sqrt{6} = 3.449490$; the four branches visible to its right are precisely the four-cycle points tabulated in Table 2. Panel (c), spanning 3.51 to 3.80, shows the cascade accumulating at 3.569946 and the transition to a regime of aperiodic bands, together with the band mergings that occur in reverse order above the accumulation point. Panel (d), spanning 3.80 to 4, is dominated by the period-three window opening at $1 + \sqrt{8} = 3.828427$, which appears as a clean vertical gap in the chaotic sea. The period-three cycle inside it undergoes its own complete period-doubling cascade, a copy of the whole diagram in miniature. This self-similarity is universality made visible, and it is why the same constant governs both.

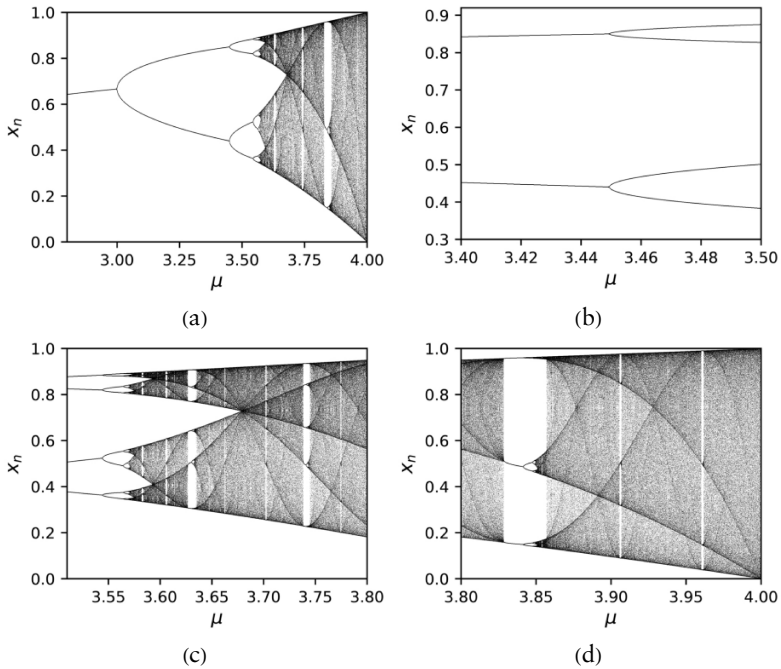


Figure 6. Bifurcation diagrams of the logistic map. Panel (a) spans μ from 2.8 to 4 and shows the cascade, with thresholds at the values of Table 4 and spacings contracting by the factor 4.669. Panel (b) spans 3.4 to 3.5 and resolves the second doubling at $1 + \sqrt{6} = 3.449490$; the four branches to its right are the cycles of Table 2. Panel (c) spans 3.51 to 3.80 and shows accumulation at 3.569946 followed by the reverse band-merging cascade. Panel (d) spans 3.80 to 4 and shows the period-three window opening at $1 + \sqrt{8} = 3.828427$, which contains a scaled copy of the entire diagram.

10.3 Conjugacy and Tent Map Figures

Figures 7 and 8 display the tent map and the logistic map at $\mu = 4$ together with their fourth iterates. The essential feature is that the fourth iterate of the tent map has $2^4 = 16$ full monotone branches, each mapping its subinterval onto the whole unit interval, and that the fourth iterate of f_4 has the same 16 branches, smoothly distorted by h. This branch count is the entire content of the periodic-point count in Proposition 2 and of the entropy ln2, since each additional iterate doubles the number of laps.

Figure 9 shows the commuting square of Theorem 4: traveling right then down gives the same map as traveling down then right.

Figure 10 places the two fourth iterates side by side so that the branch-by-branch correspondence can be counted directly.

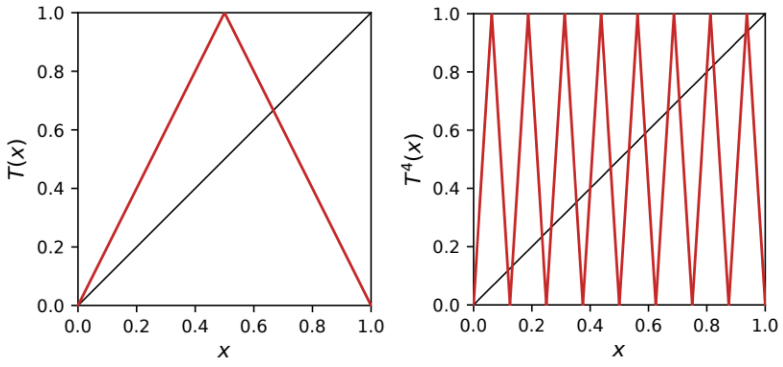


Figure 7. The tent map and its fourth iterate. Panel (a) shows T and panel (b) shows T^4, which has $2^4 = 16$ full monotone branches, each mapping a dyadic subinterval onto the unit interval. Each branch crosses the diagonal once, giving 16 points of period dividing four.

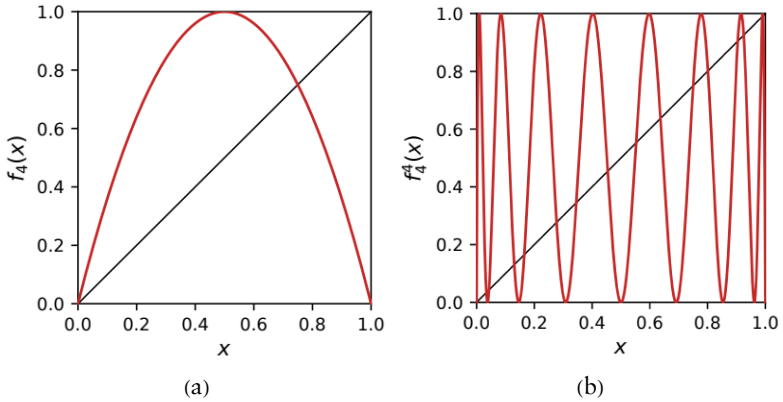


Figure 8. The logistic map at $\mu = 4$ and its fourth iterate. Panel (a) shows f_4 and panel (b) shows the fourth iterate. Comparison with Figure 7 shows that the branch count is identical, the branches being merely curved by the conjugacy.

https://doi.org/10.25088/ComplexSystems.35.3.203

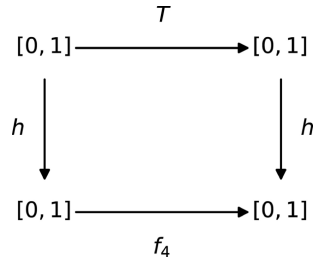


Figure 9. The commuting square of the conjugacy. Following either path around the square gives the same map, since $h \circ T = f_4 \circ h$ with $h(x) = \sin^2(\pi x/2)$, so the tent map and the logistic map at $\mu = 4$ have identical topological dynamics.

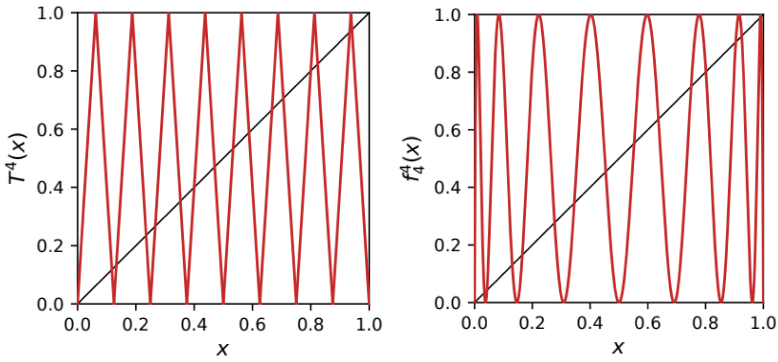


Figure 10. Direct comparison of the fourth iterates. Panel (a) shows the tent map and panel (b) the logistic map at $\mu = 4$, placed side by side so that the 16 branches can be matched one to one. The number and ordering of the branches are conjugacy invariants; only the shape differs.

10.4 Lyapunov Exponent Curves

Figure 11 shows a plot of the Lyapunov exponent against μ. Below the accumulation point, the curve is negative except at the thresholds μ_n, where it touches zero, and it carries downward spikes to $-\infty$ at each superstable parameter of Table 5. These spikes are genuine rather than artifacts, and their accumulation locates μ_∞. Above that parameter, the exponent is positive on a set of positive measure but is interrupted by the periodic windows, where it dips negative; the deepest visible dip is the period-three window at 3.828427, corresponding to the row at $\mu = 3.83$ in Table 6. The curve terminates at $\ln 2$ at $\mu = 4$, in agreement with Theorem 3, which provides an end-to-end check on the entire computation.

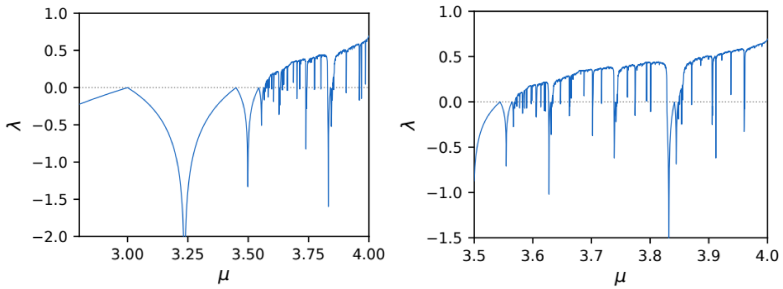


Figure 11. Lyapunov exponent of the logistic map against μ. Panel (a) spans 2.8 to 4 and panel (b) spans 3.5 to 4. Downward spikes to $-\infty$ mark the super stable parameters of Table 5, and their accumulation locates $\mu_\infty = 3.569946$. The exponent also vanishes at each threshold μ_n, so μ_∞ is not its first zero; what is specific to that parameter is that the principal chaotic bands, carrying a positive exponent, begin immediately above it. Negative dips further to the right are periodic windows, the deepest being the period-three window at 3.828427. The curve ends at $\ln 2$ at $\mu = 4$, in agreement with Theorem 3.

11. Discussion and Limitations

11.1 The Nature of the Contribution

The contribution is an integrated and independently checked exposition, not new mathematics. Every theorem stated here is classical. What has been supplied is the combination that is hard to find in one place: complete proofs at the level of a first graduate course, numerics computed to a precision at which the predictions of the theory can actually be confirmed, an explicit account of the numerical pitfalls and figures that are discussed rather than merely displayed.

The treatment has been deliberate about the points that are easy to get wrong in a compressed account, because those errors are pedagogically costly. A student who computes a ratio near 4.63 from four-decimal thresholds and cannot see why it will not converge learns the wrong lesson about numerical mathematics, and a student who is told that the fixed point is unstable at $\mu = 3$ has been given a false statement that will contradict their own experiment.

11.2 Limitations

The analysis is confined to a single one-parameter family of one-dimensional maps, and three limitations follow. First, the results say nothing directly about higher-dimensional systems, where the single Lyapunov exponent becomes a spectrum and where chaos can coexist with contraction in other directions. Second, only the quadratic family is treated; while universality gives the same constant

throughout a broad class of unimodal maps with a quadratic critical point, that theorem is neither proved here nor tested on other families. Third, the treatment of the parameter region above the accumulation point is descriptive: the windows are exhibited numerically, but neither the kneading theory that classifies them nor the theorem on the positive measure of the chaotic parameter set [10] is developed.

11.3 Directions

Three extensions would fit naturally. Kneading theory [11] would put the ordering of the windows in panel (d) of Figure 6 on a rigorous foot ing and connect it to the theorem on coexistence of cycles [8]. Verifying the universality of δ numerically across several unimodal families, of which $\mu\sin(\pi x)$ is the standard companion, would make the universality claim concrete for a reader at small computational cost. Finally, applying the same protocol to the Hénon map would introduce the two-dimensional case and the Lyapunov spectrum while reusing the machinery developed here.

12. Conclusion

A self-contained treatment of the logistic map has been given, running from the elementary stability of its fixed points to a complete proof that f_4 is chaotic in the sense of Devaney, with topological entropy and Lyapunov exponent both equal to ln2. Along the way, the period-doubling thresholds were determined to 10 significant figures, Feigenbaum scaling was exhibited from two independent sequences, the standard misstatement about the marginal parameter $\mu = 3$ was corrected, and the numerical practices on which the familiar pictures silently depend, namely transient discarding, multiplier verification, precision requirements and the limits of pointwise trajectory accuracy, were documented. The material is classical; the intended value is that it is here assembled, proved and checked in one place.

Acknowledgments

Part of this work was conducted while the author was affiliated with the Faculty of Mechanical Engineering, Brno University of Technology, Technická 2896/2, 61669 Brno, Czech Republic. The author thanks Professor Mgr. Pavel Řehák, Ph.D., and colleagues at Brno University of Technology for their support, and an anonymous reviewer, whose observation that certain table entries did not follow from the stated recurrence prompted the systematic verification reported in Section 9.

Appendix

A. Reference Implementation

The scripts given here reproduce the principal computations of the paper. Sections A.1 through A.4 are MATLAB and generate the cobweb plots, the bifurcation diagrams, the Lyapunov exponent curve and the attracting cycles of Table 2. Section A.5 gives the extended-precision routine that produced the thresholds of Table 4, written in Python with the mpmath library, since those computations were carried out at 50-digit precision even though the table reports the resulting thresholds to 10 significant figures; the superstable parameters of Table 5 are computed by the same method, with the single equation (12) in place of the pair (10). Code for the tent-map and conjugacy figures, which involve no numerical subtlety, is omitted. A single script running all of the checks reported in Section 9 is available from the author.

A.1 Cobweb Plots

```
% Cobweb plot for the logistic map.
% Reproduces Figures 1–5. Panel (a) of each figure uses x0 = 0.1
% and panel (b) uses x0 = 0.2; vary mu for the different figures.
clear; close all;
mu    = 2;      % control parameter: 2, 3, 3.22, 3.3 or 4
x0    = 0.1;    % initial condition: 0.1 for panel (a), 0.2 for panel (b)
nIter = 50;     % no transient: the transient IS the subject
f = @(x) mu .* x .* (1 - x);

x = zeros(1, nIter+1);
x(1) = x0;
for n = 1:nIter
    x(n+1) = f(x(n));
end

figure; hold on; box on;
g = linspace(0, 1, 1200);
plot(g, f(g), 'r-', 'LineWidth', 1.6);
plot(g, g,    'k-', 'LineWidth', 0.8);
for n = 1:nIter
    plot([x(n) x(n)],   [x(n)   x(n+1)], 'b-', 'LineWidth', 0.5);
    plot([x(n) x(n+1)], [x(n+1) x(n+1)], 'b-', 'LineWidth', 0.5);
end
axis([0 1 0 1]); axis square;
xlabel('x_n'); ylabel('x_{n+1}');
exportgraphics(gcf, 'Figure_2.1.pdf', 'ContentType', 'vector');
```

https://doi.org/10.25088/ComplexSystems.35.3.203

A.2 Bifurcation Diagrams

```
% Bifurcation diagrams. Reproduces all four panels of Figure 6.
% Two points of care:
%  (1) the transient is at least 1000, not 500, and longer still
%      for the magnified panels: near a threshold convergence is
%      slow and a short transient smears the branches;
%  (2) the seed is NOT 0.5. The critical point is exceptional:
%      at mu = 4 it gives 0.5 -> 1 -> 0 -> 0, so a diagram seeded
%      there shows a fixed point at its right-hand edge rather
%      than the chaotic attractor. Any generic seed avoids this.
clear; close all;

x0    = 0.400001;   % generic seed, not the critical point
nMu   = 2400;       % mu-values per panel
nPlot = 200;        % iterates plotted per mu

%           mu_min  mu_max  transient  y-limits
panels = { 2.80,  4.00,  1000, [0.00 1.00];
           3.40,  3.50,  3000, [0.30 0.92];
           3.51,  3.80,  2000, [0.00 1.00];
           3.80,  4.00,  2000, [0.00 1.00] };
names  = {'Bifur_1.1', 'Bifur_1.2', 'Bifur_1.3', 'Bifur_1.4'};

for panelIdx = 1:size(panels, 1)
    muMin = panels{panelIdx, 1};  muMax = panels{panelIdx, 2};
    nTran = panels{panelIdx, 3};  yLim  = panels{panelIdx, 4};

    mu = linspace(muMin, muMax, nMu);
    x  = x0 * ones(1, nMu);          % vectorized over mu
    for i = 1:nTran
        x = mu .* x .* (1 - x);
    end
    M = zeros(nPlot, nMu);  X = zeros(nPlot, nMu);
    for i = 1:nPlot
        x = mu .* x .* (1 - x);
        M(i,:) = mu;  X(i,:) = x;
    end

    figure;
    plot(M(:), X(:), '.', 'MarkerSize', 1, 'Color', 'k');
    xlabel('\mu'); ylabel('x_n');
    axis([muMin muMax yLim(1) yLim(2)]);
    exportgraphics(gcf, [names{panelIdx} '.pdf'], 'ContentType',
'vector');
end
```

A.3 Lyapunov Exponent

```
% Lyapunov exponent. Reproduces Figure 11.
% Notes:
%  (1) a transient is discarded before averaging;
%  (2) f'(x_i) is evaluated before updating x, following the
%      definition; the reverse order shifts the finite sum by
```

```
%      one term and shares the same limit;
%  (3) the curve uses a shorter average, which is sufficient for
%      the resolution of the plotted curve. The long averages of
%      Table 6 are for the selected parameters only: 2e6 iterations
%      at each of 2401 grid points would cost some five billion
%      updates for no visible gain.
clear; close all;
mu         = 2.8:0.0005:4;
nTransient = 1e4;
nIter      = 2e4;        % table values use 1e5 and 2e6 instead
LE = zeros(size(mu));

for k = 1:numel(mu)
    m = mu(k);  x = 0.1 + 1e-9;
    for i = 1:nTransient
        x = m*x*(1 - x);
    end
    s = 0;  c = 0;
    for i = 1:nIter
        d = abs(m*(1 - 2*x));   % derivative at x_i
        if d > 0
            s = s + log(d);  c = c + 1;
        end
        x = m*x*(1 - x);        % then advance
    end
    LE(k) = s/c;
end

figure;
plot(mu, LE, 'b-', 'LineWidth', 1); hold on;
yline(0, 'k:');
xlabel('\mu'); ylabel('\lambda');
grid on; axis([2.8 4 -2 1]);
% check: LE at mu = 4 should equal log(2) = 0.693147
```

A.4 Cycle Identification with Multiplier Test

```
% Identify the ATTRACTING cycle and verify it.
% Reproduces Table 2. Solving f^4(x) = x directly also returns
% the repelling fixed point and the repelling 2-cycle; only the
% multiplier test distinguishes them.
function [p, cyc, m] = attracting_cycle(mu)
    x = 0.4;
    for i = 1:4e5                % transient
        x = mu*x*(1 - x);
    end
    N = 1024;  orb = zeros(1, N);
    for i = 1:N
        x = mu*x*(1 - x);  orb(i) = x;
    end
    p = NaN;
    for q = [1 2 4 8 16 32]
        if max(abs(orb(1:N-q) - orb(1+q:N))) < 1e-12
            p = q;  break;
```

https://doi.org/10.25088/ComplexSystems.35.3.203

```
        end
    end
    cyc = sort(orb(1:p));
    m = prod(mu*(1 - 2*cyc));     % multiplier, equation (2)
    assert(abs(m) < 1, 'not attracting');
end
```

A.5 Period-Doubling Thresholds in Extended Precision

```
# Simultaneous solve of  f^N(x) = x  and  (f^N)'(x) = -1
# for (mu, x). This is the routine that produced Table 4.
#
# Arbitrary precision here is essential rather than a
# refinement. The differences mu_{n+1} - mu_n contract by a
# factor of about 4.67 per level, so double precision degrades
# after the fourth threshold, and a finite-difference Jacobian
# would degrade sooner still. mpmath carries 50 decimal digits
# below, and the composite is differentiated exactly through
# the product recursion for the derivative of a composite.

from mpmath import mp, mpf, findroot, sqrt

mp.dps = 50                    # 50 significant decimal digits

def orbit_and_deriv(mu, x, N):
    # returns f^N(x) and (f^N)'(x)
    d = mpf(1)
    for _ in range(N):
        d *= mu * (1 - 2*x)
        x = mu * x * (1 - x)
    return x, d

def threshold(n, mu0, x0):
    # locates mu_{n+1}: the 2^n cycle attains multiplier -1
    N = 2 ** n
    sol = findroot(
        lambda m, y: (orbit_and_deriv(m, y, N)[0] - y,
                      orbit_and_deriv(m, y, N)[1] + 1),
        (mpf(mu0), mpf(x0)))
    return sol[0]

seeds = [(3.0, 0.66667), (3.44949, 0.44), (3.5440904, 0.36),
         (3.5644073, 0.35), (3.5687594, 0.3450)]
MU = [threshold(n, m, x) for n, (m, x) in enumerate(seeds)]

for k, m in enumerate(MU, 1):
    print('mu_%d = %s' % (k, mp.nstr(m, 12)))

# exact checks on the two thresholds that are known in closed form
assert abs(MU[0] - 3)             < mpf('1e-40')
assert abs(MU[1] - (1 + sqrt(6))) < mpf('1e-40')

# ratios delta_n = (mu_n - mu_{n-1}) / (mu_{n+1} - mu_n)
for i in range(1, len(MU) - 1):
```

```
    d = (MU[i] - MU[i-1]) / (MU[i+1] - MU[i])
    print('delta_%d = %s' % (i+1, mp.nstr(d, 8)))

# Output:
#   mu_1 = 3.00000000000    mu_2 = 3.44948974278  (= 1+sqrt(6))
#   mu_3 = 3.54409035955    mu_4 = 3.56440726610
#   mu_5 = 3.56875941954
#   delta_2 = 4.7514462  delta_3 = 4.6562510  delta_4 = 4.6682422
```

References

[1] R. M. May, "Simple Mathematical Models with Very Complicated Dynamics," *Nature*, **261**(5560), 1976 pp. 459–467. doi:10.1038/261459a0.

[2] S. H. Strogatz, *Nonlinear Dynamics and Chaos: With Applications to Physics, Biology, Chemistry, and Engineering*, 2nd ed., Bolder, CO: Westview Press, 2015.

[3] S. N. Elaydi, *Discrete Chaos: With Applications in Science and Engineering*, 2nd ed., Boca Raton, FL: Chapman and Hall/CRC, 2008.

[4] R. L. Devaney, *An Introduction to Chaotic Dynamical Systems*, 2nd ed., Redwood City, CA: Addison-Wesley, 1989.

[5] R. C. Robinson, *Dynamical Systems: Stability, Symbolic Dynamics, and Chaos*, 2nd ed., Boca Raton, FL: CRC Press, 1999.

[6] M. J. Feigenbaum, "Quantitative Universality for a Class of Nonlinear Transformations," *Journal of Statistical Physics*, **19**(1), 1978 pp. 25–52. doi:10.1007/BF01020332.

[7] D. Singer, "Stable Orbits and Bifurcation of Maps of the Interval," *SIAM Journal on Applied Mathematics*, **35**(2), 1978 pp. 260–267. doi:10.1137/0135020.

[8] A. N. Sharkovskii, "Coexistence of Cycles of a Continuous Map of the Line into Itself," *Ukrainian Mathematical Journal*, **16**(1), 1964 pp. 61–71.

[9] J. Banks, J. Brooks, G. Cairns, G. Davis and P. Stacey, "On Devaney's Definition of Chaos," *The American Mathematical Monthly*, **99**(4), 1992 pp. 332–334. doi:10.2307/2324899.

[10] M. V. Jakobson, "Absolutely Continuous Invariant Measures for One-Parameter Families of One-Dimensional Maps," *Communications in Mathematical Physics*, **81**(1), 1981 pp. 39–88. doi:10.1007/BF01941800.

[11] J. Milnor and W. Thurston, "On Iterated Maps of the Interval," in *Dynamical Systems: Proceedings of the Special Year Held at the University of Maryland, College Park, 1986–87* (J. C. Alexander, ed.), Berlin: Springer, 1988 pp. 465–563. doi:10.1007/BFb0082847.